Astronomy & Astrophysics manuscript no. Submit1
April 4, 2017
©ESO 2017

Quantifying systematics from the shear inversion on weak-lensing peak counts

Chieh-An Lin[1,2] and Martin Kilbinger[1,3]

[1] Service d'Astrophysique, CEA Saclay, Orme des Merisiers, Bât 709, 91191 Gif-sur-Yvette, France
e-mail: chieh-an.lin@cea.fr
[2] Fenglin Veteran Hospital, 2 Zhongzheng Rd. Sec. 1, Fenglin Township, Hualien 97544, Taiwan
[3] Sorbonne Universités, UPMC Univ. Paris 6 et CNRS, UMR 7095, Institut d'Astrophysique de Paris, 98 bis bd Arago 75014 Paris, France

Draft version April 4, 2017

ABSTRACT

Weak-lensing (WL) peak counts provide a straightforward way to constrain cosmology, and results have been shown promising. However, the importance of understanding and dealing with systematics increases as data quality reaches an unprecedented level. One of the sources of systematics is the convergence-shear inversion. This effect, inevitable from observations, is usually neglected by theoretical peak models. Thus, it could have an impact on cosmological results. In this letter, we study the bias from neglecting the inversion and find it small but not negligible. The cosmological dependence of this bias is difficult to model and depends on the filter size. We also show the evolution of parameter constraints. Although weak biases arise in individual peak bins, the bias can reach 2σ for the dark energy equation of state $w_0^{\rm de}$. Therefore, we suggest that the inversion cannot be ignored and that inversion-free approaches, such as aperture mass, would be a more suitable tool to study weak-lensing peak counts.

Key words. Gravitational lensing: weak, Cosmology: large-scale structure of Universe, Methods: numerical

arXiv:1704.00258v1 [astro-ph.CO] 2 Apr 2017

1. Introduction

Peak counts are powerful non-Gaussian statistics that allow to constrain cosmology from weak lensing (WL). Peaks of high S/N are shown to be good tracers of massive halos (Yang et al. 2011; Lin & Kilbinger 2015a, hereafter Paper I). Accordingly, WL peak counts are sensitive to the change of shape of the mass function. In the literature, it has been shown that peak counts alone constrain cosmology more strictly than two-point-correlation functions (Dietrich & Hartlap 2010; Liu, J. et al. 2015a). Applications to observational data are also multiple. The data of the Canada-France-Hawaii-Telescope Lensing Survey have been analyzed by Liu, J. et al. (2015a) and Liu, X. et al. (2016), CFHT Stripe-82 Survey by Liu, X. et al. (2015b), and Dark Energy Survey Science Verification data by Kacprzak et al. (2016).

For future large and deep lensing surveys, the importance of dealing with systematics increases significantly. To cite a few, potential sources of systematics are shape measurement errors (Cardone et al. 2014), photometric redshift uncertainty (Cunha et al. 2014; Bonnett et al. 2016; Gruen & Brimioulle 2016; Choi et al. 2016), intrinsic alignment of galaxies (Chisari et al. 2014; Codis et al. 2015; Schaefer & Merkel 2015; Schrabback et al. 2015; Krause et al. 2016), baryon physics (Mohammed et al. 2014; Harnois-Déraps et al. 2015), and instrumental responses (Gurvich & Mandelbaum 2016; Okura et al. 2016; Kannawadi et al. 2016; Plazas et al. 2016). Studies focusing on the impact on peak counts have been done by Yang et al. (2013) and Osato et al. (2015) for baryon physics, Liu, X. et al. (2014) for masking, and Liu, J. et al. (2014) for magnification bias (see also Lin 2016 for a review on WL-peak-related studies).

One of the systematics that have not been addressed is the convergence-shear inversion. In WL, the (reduced) shear is observable but the convergence field is not. One way to obtain the convergence is to invert its relation to the shear via the lensing potential. This calculation is done in Fourier space in practice and can be contaminated by at least three realistic survey effects. First, galaxies only provide irregular samples of the field so the noise property is not uniform. Second, inversion methods cannot account for the reduced shear without nonlinear effects. Third, it is difficult to model and to propagate the impact from masking and missing data. An alternative to the inversion is to obtain the convergence via aperture mass (Kaiser et al. 1994). However, this linear filtering technique is limited to compensated filters and still needs to face to three survey effects mentioned above.

In the literature, Fan et al. (2010) and Shirasaki (2017) have proposed theoretical models for WL peaks. These models behave on the convergence field, without including the impact of the inversion [♯1]. Therefore, such approaches could lead to a bias on parameter estimation. The purpose of this letter is to quantify this bias introduced by the inversion on WL peak counts. Two algorithms, the Kaiser-Squire and Seitz-Schneider inversions, are considered in this study. We use our stochastic model developed in Paper I, Lin & Kilbinger (2015b, Paper II), and Lin et al. (2016, Paper III) to examine this effect. Its flexibility to model simultaneously peaks from a direct computation of the convergence and from the shear with the inversion makes it an ideal tool to achieve our objective.

[♯1] The model of Fan et al. (2010) can estimate peaks directly from a shear field, but it is computationally expensive.

After the introduction, the methodology is explained in Sect. 2. The results are presented in Sect. 3. Then, we will summarize the letter and conclude with a discussion in Sect. 4.

2. Methodology

We used the CAMELUS code (Paper I) to model peak-count predictions. This semi-analytical model adopts a halo approach, deriving peak number counts from fast halo simulations generated from a mass function. In this way, massives dark-matter halos are considered as the major source of WL peaks. Readers are invited to read Paper I for a more detailed description.

In this letter, we aim to test the impact of the convergence-shear inversion on WL peak counts. The most commonly used technique is the Kaiser-Squires (KS) inversion (Kaiser & Squires 1993) in which the convergence κ is given by

$$\hat{\kappa} = \frac{\ell_1^2 - \ell_2^2 - 2\mathrm{i}\ell_1\ell_2}{\ell_1^2 + \ell_2^2}\hat{\gamma} \quad \text{for } \ell_1\ell_2 > 0, \tag{1}$$

where $\hat{}$ is the Fourier transform operator and ℓ is the discrete Fourier mode. The arguments of κ and γ are omitted. To recover κ, the inverse transform leaves an undetermined constant term in direct space, corresponding to $\ell_1 = \ell_2 = 0$. This global constant is usually set to zero as the expected mean of the convergence field is null. In the WL regime, the reduced shear $g \equiv \gamma/(1-\kappa)$ which has an unbiased estimator using the observed galaxy ellipticities (Seitz & Schneider 1997) is often approximated by the shear, so that $g \approx \gamma$ and Eq. (1) is applied on g directly. To account for the factor $1/(1-\kappa)$ properly, Seitz & Schneider (1995) proposed the following iterative process:

$$\begin{aligned}
&\kappa^{(0)} = 0,\\
&\gamma^{(i)} = (1-\kappa^{(i-1)})\frac{1 - \mathrm{sign}\left(\det \mathcal{A}^{(i-1)}\right)\sqrt{1-|\delta|^2}}{\delta^*} \quad \text{for } i \geq 1, \text{ and}\\
&\hat{\kappa}^{(i)} = \frac{\ell_1^2 - \ell_2^2 - 2\mathrm{i}\ell_1\ell_2}{\ell_1^2 + \ell_2^2}\hat{\gamma}^{(i)} \quad \text{for } i \geq 1,
\end{aligned} \tag{2}$$

where $\det\mathcal{A} = (1-\kappa)^2 - |\gamma|^2$ and $\delta = 2\gamma(1-\kappa)/((1-\kappa)^2 + |\gamma|^2) = 2g/(1+|g|^2)$. In the case where $\det\mathcal{A}$ is always positive (i.e. $|g| < 1$), the second line of Eq. (2) is equivalent to $\gamma^{(i)} = (1-\kappa^{(i-1)})g$.

In order to test the impact from the convergence-shear inversion, we computed peak counts from the same CAMELUS simulation in three different cases: (1) obtained from simulated convergence fields (without inversion), (2) obtained from simulated shear fields inverted by KS inversion, and (3) obtained from simulated shear fields inverted by SS inversion. In Case 1, κ was computed directly so that the inversion is not needed. This convergence-peak modelling was adopted by Fan et al. (2010) and Shirasaki (2017). In Cases 2 and 3, the CAMELUS computed g and applied the two inversion techniques mentioned above, respectively. These two cases represent the real-world scenario. If the inversion introduces a significant bias, a comparison of Case 1 to Case 2 or 3 will be able to separate this bias from other effects. We would like to highlight again that the number counts from all three cases were derived from the same fast halo simulation with the same galaxy assignment, so that the stochasticity associated with halos and galaxies is suppressed.

For this letter, we performed two sets of fast simulations. The first is for quantifying the bias from the inversion using the following diagnostic: $(N^{\kappa}_{\mathrm{peak}} - N^{g}_{\mathrm{peak}})/N^{g}_{\mathrm{peak}}$, where $N^{\kappa,g}_{\mathrm{peak}}$ is the number of peaks obtained directly from the convergence or from the shear with inversion. The denominator is the peaks from the inverted shear since this corresponds to the observation. Implicitly, the "inversion bias" defined in this letter does not refer to "the bias caused by the inversion" but "the bias of modelling which does not account for the inversion". For this test, 2000 independent realizations were carried out for nine cosmologies varying Ω_{m} and σ_8. The second set is for measuring how cosmological constraints are affected. We mimicked the observational data vector by peaks from Case 2 under a reference cosmology $(\Omega_{\mathrm{m}}, \sigma_8, w_0^{\mathrm{de}}) = (0.28, 0.82, -0.96)$, while the likelihood was computed in both Cases 1 and 2. This second set was the same fast simulations as in Paper III, which consisted of 37536 cosmologies with 500 independent realizations each. For both sets, a realization was a 450×450 map with a pixel width of 0.8 arcmin, such that the field area was 36 deg^2. Three Gaussian filters of widths 1.2, 2.4, and 4.8 arcmin were applied.

WL peaks from Cases 2 and 3 were defined in the same way as in Paper III: shape noise was added for all galaxies which were binned later; after the inversion and the filtering, the noise level for S/N is estimated locally based on the number of neighboring galaxies. For Case 1, we first binned galaxies to derive a noise-free convergence map, then added shape noise in pixels, and finally determined S/N with a constant noise level. The motivation for this modification is to proceed the computation in the same way as analytical convergence-peak models (Fan et al. 2010; Shirasaki 2017), which are restricted to such configuration. Apart from the definition of S/N, the remaining configuration of CAMELUS was identical to Paper III.

To take into account degeneracies, the constraint contours are fitted with three indicators:

$$\Sigma_8 = \left(\frac{\Omega_{\mathrm{m}} + \beta}{1-\alpha}\right)^{1-\alpha}\left(\frac{\sigma_8}{\alpha}\right)^{\alpha}, \tag{3}$$

$$I_1 = \Omega_{\mathrm{m}} - a_1 w_0^{\mathrm{de}}, \quad \text{and} \tag{4}$$

$$I_2 = \sigma_8 + a_2 w_0^{\mathrm{de}}, \tag{5}$$

which are respectively degeneracy lines for the Ω_{m}-σ_8, σ_8-w_0^{de}, and Ω_{m}-w_0^{de} planes. This definition of Σ_8 allows a good measurement of contour width independent from α. Equations (4) and (5) assume that w_0^{de} is connected to two other considered parameters by an affine relation. An analysis of these indicators allows to examine how degeneracy lines vary. Here, we set $\alpha = 1/3$, $\beta = 0$, $a_1 = 0.108$, and $a_2 = 0.128$ and computed the fitted Σ_8, I_1, and I_2 respectively in Cases 1 and 2. This choice of α and β makes Σ_8 a functional form similar to $\sigma_8\Omega_{\mathrm{m}}^{0.5}$; and the choice of a_1 and a_2 is the best fit result taken from Paper III.

3. Results

Figure 1 shows the peak function from the reference cosmology $(\Omega_{\mathrm{m}}, \sigma_8, w_0^{\mathrm{de}}) = (0.28, 0.82, -0.96)$ with the filter of 2.4 arcmin, using the first simulation set mentioned in Sect. 2. Blue circles, red squares, and green diamonds respectively show the mean peak density over 2000 realizations in three studied cases. The error bars are rescaled to correspond to a survey of 1080 deg^2. We see that the biases of the convergence case compared to both shear cases are relatively small. They are globally contained with in ±30% of Cases 2 and 3. The difference between the KS and SS inversions is even smaller, revealing that the inversion method has little importance on peaks.

We observe that high and low peaks do not seem to have the same variation. In Fig. 1, the convergence modelling underestimates the number of low peaks and overestimates high ones.

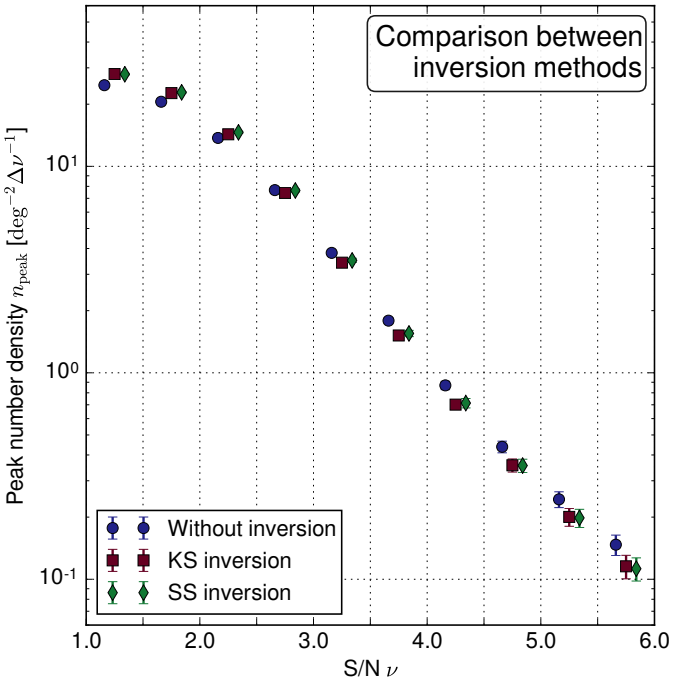

Fig. 1. Peak function from different studied cases. The filter size is 2.4 arcmin. The input cosmology is $(\Omega_{\rm m}, \sigma_8, w_0^{\rm de}) = (0.28, 0.82, -0.96)$. We can see that the impact of not modelling the inversion is small. Between two inversion techniques, there is practically no difference. This plot also shows that the inversion decreases the peak counts under this configuration. However, we find that this can not be generalized for all cosmologies and all filter sizes.

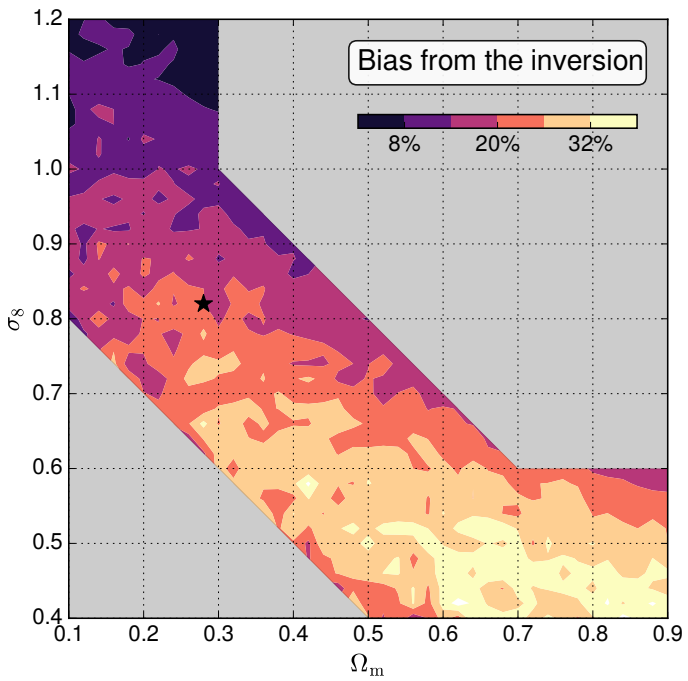

Fig. 2. Bias map under a wide range of cosmological parameters. For this figure, the KS inversion is applied. The dark energy equation of state is $w_0^{\rm de} = -0.96$, the filter size is 2.4 arcmin, and the S/N bin is $\nu = [4.0, 4.5[$. Contours of parameters sharing the same bias level can be clearly observed. However, by examining other choices of filters and bins, we observe that not only the bias levels but the contour shapes change.

Table 1. Inversion bias obtained under different cosmologies. We recall that the bias is defined as $(N^{\kappa}_{\rm peak} - N^{g}_{\rm peak})/N^{g}_{\rm peak}$. This table represents the bin $\nu \in [4.0, 4.5[$. The dependence of the bias on cosmology is not trivial.

$\Omega_{\rm m}$	σ_8	KS inversion			SS inversion		
		G1.2	G2.4	G4.8	G1.2	G2.4	G4.8
0.23	0.77	12.8%	27.0%	3.4%	19.6%	24.8%	-0.2%
0.28	0.77	16.4%	23.6%	6.4%	23.1%	21.9%	3.4%
0.33	0.77	19.0%	24.0%	6.7%	25.7%	22.7%	3.6%
0.23	0.82	15.4%	22.9%	5.5%	22.6%	21.4%	2.4%
0.28	0.82	18.3%	23.9%	5.4%	25.2%	21.8%	2.5%
0.33	0.82	18.2%	19.7%	3.1%	24.5%	19.0%	0.9%
0.23	0.87	16.1%	19.6%	1.5%	22.3%	18.5%	-1.9%
0.28	0.87	18.1%	21.1%	4.8%	24.7%	20.1%	2.7%
0.33	0.87	19.0%	17.7%	4.7%	24.1%	16.4%	3.2%

However, their amplitude depends on the applied filter. This is shown more clearly in Table 1 where the peak-count bias in a specific bin $\nu \in [4.0, 4.5[$ with all three filter sizes and both inversion methods are presented. Neglecting the inversion effect does not affect the bias in the same way for different filters, and we find the same ambiguity for other S/N bins which are not shown.

Table 1 also shows an ambiguous dependence on cosmology. It is not clear that high $\Omega_{\rm m}$ or high σ_8 would yield a larger or smaller bias. To visualize better the cosmological dependence of the bias, we computed the bias for each cosmology from the second fast simulation set (Sect. 2) and obtained a "bias map" for the KS inversion (Case 1 compared to Case 2). For example, the bias map for the bin $\nu \in [4.0, 4.5[$ and the filter size of 2.4 arcmin is presented in Fig. 2. Although noisy, the contours of bias levels are visible, and within the studied range of cosmologies, the bias can vary from 2% to 38%. This figure shows the complex dependence of the peak-count bias on cosmology. Moreover, when we draw the bias maps for other bins and filter sizes, both contour shape and value range vary a lot. This variation is difficult to explain. In some cases, like in Fig. 2, elliptical contours seem to form; in others cases, we only see degeneracy lines. In the end, we argue that cosmology affects the inversion bias in a very complex way which depends on the filter size and the bin range at least.

Table 2. Diagnostics of cosmological constraints. The indicators Σ_8, I_1, and I_2

Constraints	$\Omega_{\rm m}$-σ_8	$\Omega_{\rm m}$-$w_0^{\rm de}$	σ_8-$w_0^{\rm de}$
Indicator	Σ_8	I_1	I_2
Case 1 (convergence)	$1.03^{+0.03}_{-0.04}$	$0.22^{+0.07}_{-0.04}$	$0.90^{+0.04}_{-0.15}$
Case 2 (inverted shear)	$1.09^{+0.02}_{-0.03}$	$0.37^{+0.15}_{-0.07}$	$0.64^{+0.14}_{-0.11}$

How does the inversion bias affect cosmological constraints? Figure 3 shows a comparison where solid and dashed contours are obtained from the inverted shear of Case 2 and shaded areas from Case 1. More precisely, contours correspond to a case where the inversion has been properly considered, while shaded areas are interpreted as from a simplified modelling which ignores the inversion effect. Although the bias in individual bins is relatively small as shown in Fig. 1, the impact on constraints is not negligible. While the $\Omega_{\rm m}$-σ_8 constraint shifts approximately along the degeneracy line, both joint constraints with $w_0^{\rm de}$ are more affected, resulting in a biased estimation of parameters. For example, the reference parameter $(\Omega_{\rm m}, w_0^{\rm de}) = (0.28, -0.96)$ has been excluded at 2σ on the left-bottom panel of Fig. 3.

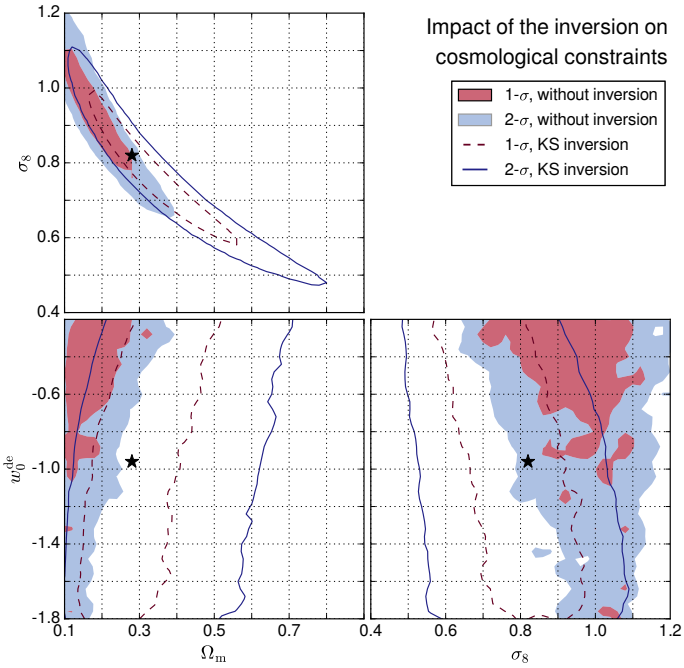

Fig. 3. Impact of the inversion bias on Ω_m-σ_8-w_0^{de} constraints. Solid and dashed lines represent contours derived from the inverted shear, whereas shaded areas from the convergence. Although the bias in individual bins is relatively small, the shift of contours is not negligible.

The shift of contours observed above are quantified by the diagnostics mentioned in Sect. 2. The values of indicators are shown in Table 2. On the plane Ω_m-σ_8, Table 2 shows that both cases exclude each other mutually by 2σ whereas Fig. 3 does not suggest such a result. This is due to a bad fitting of Σ_8 when the dragging parameter β is not relaxed. However, for the two other planes, not considering the inversion bias does yield a 2σ tension compared to the realistic case, which justifies that w_0^{de} is more affected. Knowing that the bias depends on the S/N bin and the filter size in a non-trivial way, readers should keep in mind that another choice of the data vector might yield a contour shift different from what we have observed. In the end, the inversion bias is not completely negligible in cosmological constraints.

4. Summary and discussion

In this letter, we performed fast simulations with CAMELUS to quantify the effect of neglecting the convergence-shear inversion in WL peak-count modelling. On the one hand, we simulated the shear signal as from observations and applied two inversion methods; on the other hand, we simulated directly the convergence signal to count the number of peaks as analytical models do. The comparison of the two yielded an estimation of how convergence modelling ignoring inversion effects would deviate from the truth.

We have found that not accounting for the inversion has a weak effect on WL peak counts, and that the difference between the KS and SS inversion methods is also small. For the reference cosmology, the bias from neglecting the inversion is contained within about 30%. However, its dependence on the S/N value, the filter size, or cosmology is not trivial and cannot be summarized as several simple rules or tendencies.

When we compared cosmological constraints between using either the convergence or the inverted shear, we found that contours can exclude each other by 2σ and that w_0^{de} is more affected while the Ω_m-σ_8 contour moves approximately along the degeneracy line. However, we would like to stay cautious before generalizing these observations. They could only be valid with the configuration of this letter since the inversion bias could vary a lot when the filter sizes change. In the end, the impact of the inversion bias is not negligible and is difficult to model.

Thus, for the future WL surveys aiming for constraining cosmological parameters with high precisions, an ideal strategy for peak-count analyses would be using the aperture mass (e.g. Dietrich & Hartlap 2010; Martinet et al. 2015). This technique bypasses the inversion and gives a convergence field filtered with compensated filters. In addition, we have already argued in Paper III that compensated filters are more strategic for combining multiscale information, since they only capture information of characteristic halo masses and are more sensitive to the change of shape of the mass function. As a result, the aperture mass is highly recommended for the purpose of studying weak-lensing peak counts.

Acknowledgements. The authors would like to thank for the financial supports from the DIM-ACAV thesis fellowship of Région d'Île-de-France and the French national program for cosmology and galaxies (PNCG), and the computing support from the in2p3 Computing Centre. We also thank Zuhui Fan and Xiangkun Liu for discussions about this letter. Linc is grateful to François Lanusse and Sandrine Pires for discussions on the build-up of tests used in this letter, and to Marie Gay for her endless helps on technical issues.

References

Bonnett, C., Troxel, M. A., Hartley, W., et al. 2016, Phys. Rev. D, 94, 042005
Cardone, V. F., Martinelli, M., Calabrese, E., et al. 2014, MNRAS, 439, 202
Chisari, N. E., Mandelbaum, R., Strauss, M. A., Huff, E. M., & Bahcall, N. A. 2014, MNRAS, 445, 726
Choi, A., Heymans, C., Blake, C., et al. 2016, MNRAS, 463, 3737
Codis, S., Gavazzi, R., Dubois, Y., et al. 2015, MNRAS, 448, 3391
Cunha, C. E., Huterer, D., Lin, H., Busha, M. T., & Wechsler, R. H. 2014, MNRAS, 444, 129
Dietrich, J. P. & Hartlap, J. 2010, MNRAS, 402, 1049
Fan, Z., Shan, H., & Liu, J. 2010, ApJ, 719, 1408
Gruen, D. & Brimioulle, F. 2016, ArXiv e-prints [arXiv:1610.01160]
Gurvich, A. & Mandelbaum, R. 2016, MNRAS, 457, 3522
Harnois-Déraps, J., van Waerbeke, L., Viola, M., & Heymans, C. 2015, MNRAS, 450, 1212
Kacprzak, T., Kirk, D., Friedrich, O., et al. 2016, MNRAS, 463, 3653
Kaiser, N. & Squires, G. 1993, ApJ, 404, 441
Kaiser, N., Squires, G., Fahlman, G., & Woods, D. 1994, in Clusters of Galaxies, ed. F. Durret, A. Mazure, & J. Tran Thanh Van, 269
Kannawadi, A., Shapiro, C. A., Mandelbaum, R., et al. 2016, PASP, 128, 095001
Krause, E., Eifler, T., & Blazek, J. 2016, MNRAS, 456, 207
Lin, C.-A. 2016, ArXiv e-prints [arXiv:1612.04041]
Lin, C.-A. & Kilbinger, M. 2015a, A&A, 576, A24
Lin, C.-A. & Kilbinger, M. 2015b, A&A, 583, A70
Lin, C.-A., Kilbinger, M., & Pires, S. 2016, A&A, 593, A88
Liu, J., Haiman, Z., Hui, L., Kratochvil, J. M., & May, M. 2014, Phys. Rev. D, 89, 023515
Liu, J., Petri, A., Haiman, Z., et al. 2015a, Phys. Rev. D, 91, 063507
Liu, X., Li, B., Zhao, G.-B., et al. 2016, Physical Review Letters, 117, 051101
Liu, X., Pan, C., Li, R., et al. 2015b, MNRAS, 450, 2888
Liu, X., Wang, Q., Pan, C., & Fan, Z. 2014, ApJ, 784, 31
Martinet, N., Bartlett, J. G., Kiessling, A., & Sartoris, B. 2015, A&A, 581, A101
Mohammed, I., Martizzi, D., Teyssier, R., & Amara, A. 2014, ArXiv e-prints [arXiv:1410.6826]
Okura, Y., Petri, A., May, M., Plazas, A. A., & Tamagawa, T. 2016, ApJ, 825, 61
Osato, K., Shirasaki, M., & Yoshida, N. 2015, ApJ, 806, 186
Plazas, A. A., Shapiro, C., Kannawadi, A., et al. 2016, PASP, 128, 104001
Schaefer, B. M. & Merkel, P. M. 2015, ArXiv e-prints [arXiv:1506.07366]
Schrabback, T., Hilbert, S., Hoekstra, H., et al. 2015, MNRAS, 454, 1432
Seitz, C. & Schneider, P. 1995, A&A, 297, 287
Seitz, C. & Schneider, P. 1997, A&A, 318, 687
Shirasaki, M. 2017, MNRAS, 465, 1974
Yang, X., Kratochvil, J. M., Huffenberger, K., Haiman, Z., & May, M. 2013, Phys. Rev. D, 87, 023511
Yang, X., Kratochvil, J. M., Wang, S., et al. 2011, Phys. Rev. D, 84, 043529